Improved Gravity Field of the Moon from Lunar Prospector

A. S. Konopliv, *et al.*

Science **281**, 1476 (1998);
DOI: 10.1126/science.281.5382.1476

tional way of mapping the distribution of these elements. The maps define three distinct rock types and regions: (i) The Fe- and Ti-rich mare basalts; (ii) rocks of intermediate Fe and Ti contents that make up the floor of the South Pole–Aitken basin and the mountainous rims of the nearside circular maria and (iii) Fe- and Ti-poor anorthositic rocks of the highlands (*7*).

A comparison of the thermal neutron data on the Fe and Ti concentrations (*7*) and those produced from Clementine spectral data (*2*) show that while the correlations are good, there are discrepancies, especially in the rim area of Mare Imbrium. These discrepancies may be due to the presence of high amounts of Sm and Gd (rare earth elements with exceptionally large neutron absorption cross sections) in the KREEP-rich deposits of Imbrium ejecta (Table 1).

The LP mission is also mapping the lunar gravity (*10*) and magnetic (*11*) fields. Before the LP mission, no spacecraft had been in low polar orbit. Hence we did not have an accurate gravity map of the moon. Gravity data provide information of crustal and upper mantle structure by delineating areas of the crust with anomalous density. They are also needed to calculate the fuel requirements for the orbital mapping portion of the mission. LP calculates the gravity field by accurately tracking how the orbit of the spacecraft is perturbed (the Doppler gravity experiment). The magnetic data will reveal the distribution and strengths of the numerous small magnetic fields of the moon. These data will allow us to determine how the magnetic fields formed and possibly help to delineate deposits of useful resources. Together, the gravity and magnetic data can be used to infer the size of the suspected lunar Fe core. Although thought to contain less than a few percent of the lunar mass (as compared to Earth's core, which contains 30% of Earth's mass), the exact size of the core provides an important constraint on how the moon formed.

The magnetic maps to date (*11*) show that strong magnetic fields fill the antipodal regions of the Mare Imbrium and Mare Serenitatis basins. The magnetic fields antipodal to Imbrium are strong enough to form the smallest known magnetosphere, magnetosheath and bow shock system in the solar system. These results support the hypothesis that shock remnant magnetization of lunar rocks was associated with the large basin forming impacts early in lunar history (*11*).

Two weeks after LP achieved its mapping orbit, the data needed to define the lunar gravity field for operational purposes were obtained. The gravity data show that to maintain a 100 ± 20 km altitude orbit, a maneuver is required every 56 days; the velocity change required is 0.22 m/s per day. The gravity data have also been used to improve the mapping of previously known nearside lunar mass concentrations (mascons), revealed three new mascons in the limb regions of the nearside, and partially resolved four new mascons on the farside. The data imply that the moon does have a small Fe-rich core of about 300 km radius (*10*).

Finally, LP will map the frequency and locations of gas release events by detecting gaseous Rn and its daughter nuclei with the alpha particle spectrometer. This mapping program will help determine the current level of lunar tectonic and post-volcanic activity. Also, because other gasses such as N_2, CO_2, and CO, which are essential for life support, may be released with the Rn, the maps may indicate where these resources may be obtained for future human activities on the moon.

The alpha particle data analysis has been complicated because large fluxes of solar alpha particles have been detected during increasingly frequent solar energetic particle events. Solar events have been occurring over half of the time since the analysis began, and the flux of alpha particles has increased during the storms by up to 3300 times the normal flux. Therefore, these results are not yet available.

References and Notes

1. W. Benz, W. L. Slattery, A. G. W. Cameron, *Icarus* **66**, 515 (1986); R. M. Canup and L. W. Esposito, *ibid.* **119**, 427 (1996); A. G. W. Cameron, *ibid.* **126**, 126 (1997).
2. P. G. Lucey, G. J. Taylor, E. Malaret, *Science* **268**, 1150 (1995).
3. D. T. Blewett, P. G. Lucey, B. R. Hawke, B. L. Jolliff, *J. Geophys. Res.* **102**, 16319 (1997); P. G. Lucey, D. T. Blewett, B. R. Hawke, *ibid.* **103**, 3679 (1998).
4. S. Nozette *et al.*, *Science* **274**, 1495 (1996).
5. Discovery missions are managed by the Principal Investigator (PI, the author) who leads a science team of Co-Investigators (Co-Is), a NASA Center Partner (Ames Research Center) and an Industry Partner (Lockheed Martin). NASA Headquarters' role is limited to that of overall management, but with minimum oversight, review, and program control. The LP science team consists of the PI and five Co-Is: M. Acuna, W. Feldman, L. Hood, A. Konopliv, and R. Lin. LP has a total budget of $63 million and was developed in only 22 months. Its cost is about one-third that of the other six current and past Discovery missions and is about 10% of the cost of earlier NASA lunar and planetary exploration missions.
6. D. J. Lawrence *et al.*, *Science* **282**, 1484 (1998).
7. W. C. Feldman *et al.*, *ibid.*, p. 1489.
8. R. C. Elphic *et al.*, *ibid.*, p. 1493.
9. W. C. Feldman *et al.*, *ibid.*, p. 1496.
10. A. S. Konopliv *et al.*, *ibid.*, p. 1476.
11. R. P. Lin *et al.*, *ibid.*, p. 1480.

12. I thank all the volunteers of Lunar Exploration, Inc., the Space Studies Institute, and the National Space Society who worked for over 6 years to make LP a reality, the small team of dedicated Lockheed Martin engineers who refined the original LP spacecraft design and then built, tested, and prepared LP for launch in 22 months, the LP science team engineers who built the science instruments, the various vendors who supplied critical hardware in record time, Spaceport Florida for preparing the launch facility, the Lockheed Martin Athena 2 launch vehicle team for insuring that LP was properly launched, the Thiokol team, who made the TLI stage, the Goddard Space Flight Center team, who do the trajectory analysis, the Deep Space Network, and the command and control teams. LP is supported by NASA.

15 June 1998; accepted 14 August 1998

Improved Gravity Field of the Moon from Lunar Prospector

A. S. Konopliv, A. B. Binder, L. L. Hood, A. B. Kucinskas, W. L. Sjogren, J. G. Williams

An improved gravity model from Doppler tracking of the Lunar Prospector (LP) spacecraft reveals three new large mass concentrations (mascons) on the nearside of the moon beneath the impact basins Mare Humboltianum, Mendel-Ryberg, and Schiller-Zucchius, where the latter basin has no visible mare fill. Although there is no direct measurement of the lunar farside gravity, LP partially resolves four mascons in the large farside basins of Hertzsprung, Coulomb-Sarton, Freundlich-Sharonov, and Mare Moscoviense. The center of each of these basins contains a gravity maximum relative to the surrounding basin. The improved normalized polar moment of inertia (0.3932 ± 0.0002) is consistent with an iron core with a radius of 220 to 450 kilometers.

The gravity field of the moon has been investigated since 1966 when the Russian Luna 10 was placed in orbit around the moon and provided dynamical proof that the oblateness of the moon's gravitational potential (*1*) was larger than the shape predicted from hydrostatic equilibrium. Soon thereafter, Muller and Sjogren (*2*) differentiated the Doppler residuals from Lunar Orbiter (LO)–V to produce a nearside gravity map that displayed sizable positive gravity anomalies within the large circular mare basins. These positive anomalies, located in nearside equatorial regions with low topography, showed areas with mass concentrations (or "mascons") in the lunar interior. Inherent in the mascons—as buried, mostly uncompensated mass anomalies—is information on the impact pro-

A. S. Konopliv, A. B. Kucinskas, W. L. Sjogren, J. G. Williams, Jet Propulsion Laboratory, California Institute of Technology, Pasadena, CA 91109, USA. A. B. Binder, Lunar Research Institute, Gilroy, CA 95020, USA. L. L. Hood, University of Arizona, Lunar and Planetary Laboratory, Tucson, AZ 85721, USA.

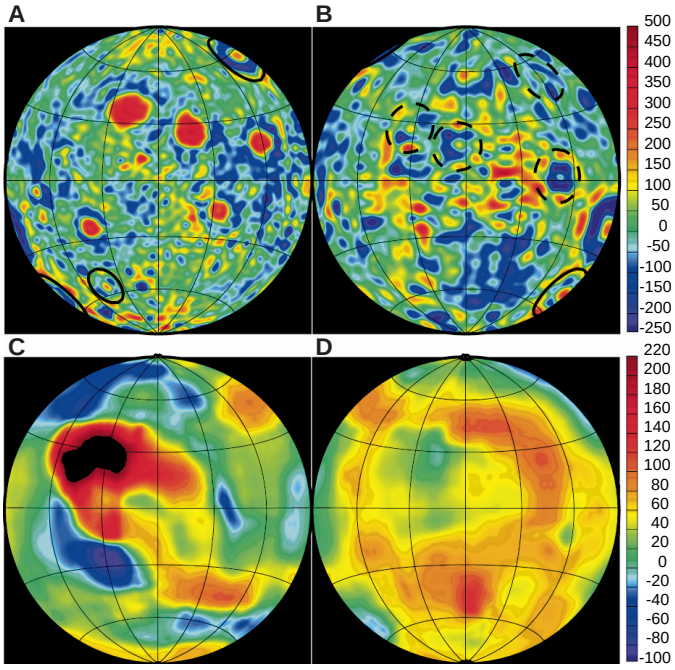

Fig. 1. Vertical gravity anomalies from LP75G at the reference surface of the moon for the (**A**) nearside and (**B**) farside with a Lambert equal-area projection. The accelerations are in milligals (1 mgal = 10^{-5} m/s^2) and represent the deviation from a uniform sphere with the J_2 contribution to the oblateness also removed. The central mass acceleration is 160,000 mgal, and the range of the deviations is about 900 mgal (~0.5% of the total). The new nearside mascon basins are denoted with solid circles and the new farside mascons with dashed circles. Crustal thickness (TT) in kilometers with an Airy compensation model for the nearside without the five principal mascons (**C**) and for the farside (**D**) shows the lunar dichotomy. Procellarum Basin (black region with $TT > 220$ km at 50°W, 20°N) and the center of South Pole–Aitken Basin are areas of maximum Airy depth.

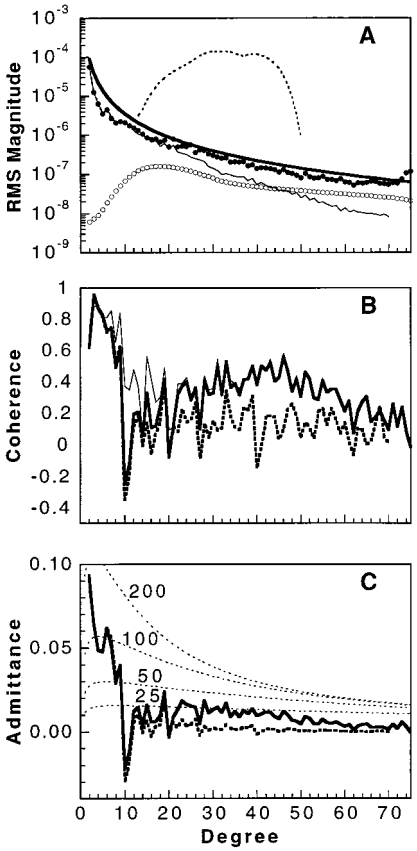

Fig. 2. (**A**) Amplitude spectrum of the lunar gravity field. Thick solid line, the expected power law ($3.5 \times 10^{-4}/n^2$); thin solid line, from GLGM2 (*3*); solid circles, from LP75G (this paper); open circles, the errors in the spectrum for LP75G; and dashed line, the spectrum from an unconstrained 50th-degree gravity solution. RMS, root mean square. (**B**) The coherence of the topography (*12*) and gravity for LP75G (thick solid line), GLGM2 (dashed line), and LP75G with the five principal mascons removed (thin solid line). (**C**) Admittance between topography and gravity field LP75G (solid line) and GLGM2 (thick dashed line). The thin dashed lines represent theoretical admittance for Airy isostatic compensation at the depths (in kilometers) indicated.

cess and the past thermal history of the moon, where the latter is inferred through the strength of the lithosphere. In addition to LO-I through -V, most of the gravity mapping of the moon was done by the Apollo 15 and 16 subsatellites and the recent Clementine mission (*3*). The Clementine data, from an elliptical orbit with a higher periapse altitude of 400 km than previous missions, improved the low degree ($n = 2$, 3) and sectoral terms (to degree 20) of the gravity field. The Clementine laser altimetry data provided the global shape of the moon, which together with the gravity, improved the physical modeling of the moon (*4*).

Lunar Prospector (LP) is in a circular polar orbit with a low 100-km altitude (*5*). The gravity information comes from tracking the spacecraft with the Deep Space Network in California, Spain, and Australia and thus measuring the line-of-sight velocity from the Doppler shift to an accuracy of 0.2 mm/s for 10-s intervals (or one part in 10^7). The lunar farside gravity field is poorly determined because the spacecraft is not in view from Earth when it is over the lunar farside. However, some information is obtained by observing changes in the LP orbit due to the accumulated acceleration of the farside gravity as the spacecraft comes out of the occultation (*6*).

The first 3 months of data from continuous tracking of LP were combined with the data from LO, Apollo, and Clementine to produce a 75th-degree and -order spherical harmonic gravity model (*7*). While solving for the gravity field (*8*, *9*), the last few degrees of the solution were corrupted by unmodeled gravity beyond degree 75. Also, the lack of farside tracking contributes noise to the gravity solution. For this reason, the global gravity (Fig. 1) contains the acceleration at the lunar surface truncated at degree 70 for the nearside and degree 50 for the farside. Our model shows features, including many small craters, to a half-wavelength resolution of 75 km, although the nearside data support a higher resolution of about 50 km and the farside resolution is about 200 km. Evident on the nearside of the moon are the five principal mascons from the mare-filled impact basins Imbrium (20°W, 37°N), Serenitatis (18°E, 26°N), Crisium (58°E, 17°N), Humorum (39°W, 24°S), and Nectaris (33°E, 16°S), as well as smaller mascons that were known from previous missions (*2*).

The roughness of the lunar gravity field is given by the amplitude of the gravity coefficients versus degree (or n) (Fig. 2A). For Earth and Venus, the spectrum has empirically been shown to follow a power law f/n^2 (*8*) with the constant f scaled for each planet to allow the same amount of global stress. For the moon to have the same amount of stress as Earth, the leading constant f is 3.5×10^{-4}. However, the measured spectrum of $1.2 \times 10^{-4}/n^{1.8}$ indicates that the moon is closer to equilibrium than Earth (*10*, *11*). The spectrum is reliable to about degree 20, but beyond that, the uncertainty in the spectrum is greater than the signal because of the lack of farside data. The true signal for the higher degrees is not expected to be much greater than our model because it nearly matches a gravity field strictly from uncompensated topography.

With a gravity data set that is closer to global, the coherence (or correlation) with topography (*12*) has also increased (Fig. 2B) for the midwavelength frequencies ($n = 20$ to 50), and global compensation (Fig. 2C) is more apparent than previous models (*4*) for this frequency range. The anticorrelation of gravity and topography, due in part to the five principal nearside mascons, is evident in degrees 10 to 20, and the tailing of the correlation at high degree is probably due to the limited topographic sampling for those frequencies (60 km between altimetry tracks) and reduction in farside gravity information.

The mascons known before LP were all on the nearside of the moon close to the equator and were filled with maria several kilometers thick (*13*). With the new LP data, seven new large mascons were identified where there is a clear maximum in the gravity at the center of each basin relative to the rest of the surrounding basin. Of the three new mascons on the nearside of the moon (see Fig. 3), Mare Humboltianum (80°E, 57°N) has lava fill, Mendel-Rydberg (95°W, 50°S) has some mare fill and possibly more covered by Mare Orientale ejecta (*14*), and Schiller-Zucchius (45°W, 55°S) shows no evidence of mare fill. Of the four new mascons on the farside of the moon, only Mare Moscoviense (147°E, 27°N) has mare fill, the others being Hertzsprung (130°W, 2°N), Coulomb-Sarton (120°W, 51°N), and Freundlich-Sharonov (175°E, 18°N). The amplitudes of the farside mascons have large uncertainties. Currently, the differences between the negative basin ring and the maximum in the basin center (100 to 150 mgal) are about one-half to one-third of the ranges for the non–mare-filled nearside mascon basins, and these nearside differences indicate that the farside amplitudes may be underestimated by a factor of 3. The nearside mascons are well determined with amplitude uncertainties of about 20 mgal.

Several processes have been proposed to explain the formation and support mechanism of lunar mascons (*10*, *15*). After a giant impact, according to one scenario, the extensive excavation of lunar material resulted in crater relaxation, a strong thermal anomaly, and high amounts of stress within the crust (*16*). The heating and weakening of the crust allowed an upwelling of denser mantle material, resulting in excess mass near the center of the basin (*17*–*19*). This mantle rebound resulted in uplift of the crust-mantle boundary (or Moho) and the formation of a dense mantle "plug." At this time, the basins were in near isostatic equilibrium, but a deep topographic depression remained. Subsequently, the remaining depression in the basin was filled with flood basalts. This filling left the mascons as uncompensated buried loads (excess mass) in the basins.

Thus, the mascon anomalies are the result of the combination of the dense mantle plug and the basin fill (*20*). However, in the context of this model, the question of the respective contribution of mantle plug and subsequent mare fill to the observed positive mascon gravity anomaly is a matter of debate. Some believe that the mare fill is of relatively low density and that most of the positive mascon anomaly is due to the high-density mantle plug (*17*). Others argue that the mass anomalies responsible for the five principal mascons (in particular, Mare Serenitatis) are thin and near the surface with the dominant contribution coming from a high-density mare fill (relative to the crust) rather than a mantle plug (*18*). Their argument stems from the strong shoulders seen in the line-of-sight Doppler data. Likewise, the gravity model presented here does show a plateau for the principal mascons (see Fig. 4) not seen in the Goddard Lunar Gravity Model–2 (GLGM2) model (*3*). The LP extended mission with 10- to 40-km altitude will provide further data to separate out the contributions of maria and mantle plug.

Analysis of the new mascons will also help the debate on mantle rebound. Following a suggestion by Taylor (*21*), Neumann *et al.* (*22*) hypothesized a dynamic rather than long-term isostatic adjustment mechanism of mantle upwelling. In their view, the mascon anomalies are essentially due to a combination of rapid mantle rebound, immediately after and a direct cause of the basin-forming impact, and an additional mass excess component from the mare basalt filling that was emplaced at a later date. Arkani-Hamed (*15*, *23*) proposes an active mascon formation model, relating mascon formation directly to the effect of giant impacts. In this hypothesis, partial melting occurs beneath the surrounding highlands as a consequence of thermal blanketing by the ejecta; molten basalt is then laterally transported from beneath the highlands into the basins. Arkani-Hamed further proposes a viscous decay model for support of the mascons, emphasizing the role of viscous deformation of the lunar interior. He argues that the elastic layer of the moon was not thick enough to achieve mascon support at the time of their formation near 3.6 billion years ago (*24*). Elastic support was achieved at a later date (about 3 billion years ago) when the upper parts of the moon became strong enough. However, studies of mascon anomalies corrected for mare fill estimates (*13*) seem to suggest that basins were supporting stress before mare filling (*22*). In this view, support of the mascons would have been achieved through flexural stresses not long after formation (*25*).

We produced an Airy isostasy (isostatic compensation through a low-density root) crustal thickness map for the moon without making the a priori assumption of a fixed thickness for the lunar background (or reference) crustal thickness (*4*, *22*, *26*). This map allows us to test the physical validity of the Airy model for a given region in addition to showing global trends in Airy crustal thickness variations. The map of the regional Airy crustal thickness (Fig. 1, C and D) was obtained with spatial domain Geoid-Topography Ratio (GTR) techniques (*27*) with the Clementine topography (*12*) and our gravity with the five principal mascons removed with negative mass sheets at 50-km depth. For each fixed position of the sliding window, mean values of the spherical harmonic–derived geoid anomaly (*N*) and topography

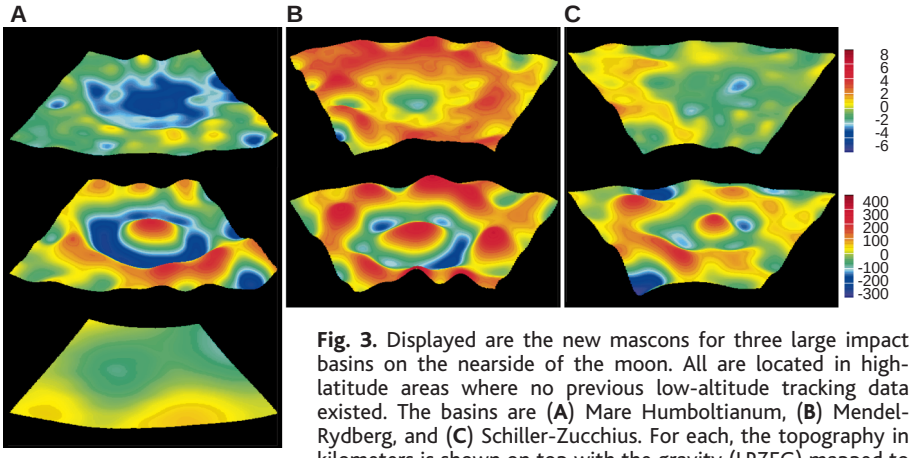

Fig. 3. Displayed are the new mascons for three large impact basins on the nearside of the moon. All are located in high-latitude areas where no previous low-altitude tracking data existed. The basins are (**A**) Mare Humboltianum, (**B**) Mendel-Rydberg, and (**C**) Schiller-Zucchius. For each, the topography in kilometers is shown on top with the gravity (LP75G) mapped to the surface shown beneath it. For comparison, the gravity before LP (*3*) is also shown in the bottom panel of (A). The gravity central peak at the center of each basin is evident and corresponds to the topographic low.

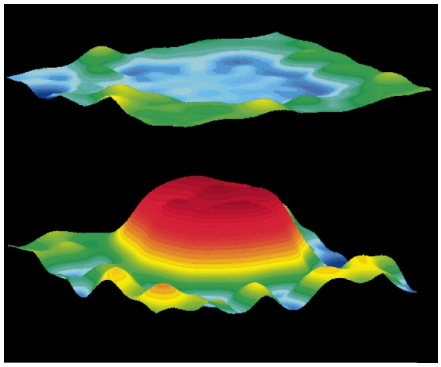

Fig. 4. Topography (**top**) and surface gravity (**bottom**) for Mare Serenitatis. The gravity shows a plateau and thus a substantial near-surface contribution to the mascon. Also apparent is the smaller mascon Mare Vaporum in the lower left and center part of the figure. Color bar scales are the same as for Fig. 3.

variation (h) are compared, in the least squares sense and in the spatial domain, with theoretical Airy correlations of N and h. This comparison results in a best fit value of the reference crustal thickness H for the region within the window. This value is then added to the mean h and corresponding value of the Airy root (b) to produce a total mean crustal thickness TT for the region within the data window [$TT(h) = h + b(h) + H$].

In reasonable agreement with previous studies (*22*), we find that Airy compensation may be a viable model for the highlands, with a mean Airy reference crustal thickness of about 70 km. When the gravity data include all mascons, the GTR results yield a large negative compensation depth for the lowland mascon basins. This result suggests that one-layer Airy isostasy is not valid in these areas, a concern already addressed by other authors (*26*). With the five mascons removed (Fig. 1), the lowland basins display more realistic Airy crustal thickness, closer, for some basins, to results obtained with other techniques (*4*, *22*). There are large positive Airy crustal thickness anomalies in the South Pole–Aitken basin and Procellarum basin. These basins do not have mascons, and the thickness anomalies may be related to Pratt isostasy (lateral variations in crustal density).

Because LP is a simple spin-stabilized spacecraft, it is ideal for long-wavelength gravity studies because of limited nonconservative forces acting on the spacecraft. The resulting unnormalized second-degree values of interest are gravitational coefficients $J_2 = (203.428 \pm 0.09) \times 10^{-6}$ and $C_{22} = (22.395 \pm 0.015) \times 10^{-6}$, where errors are five times the formal statistics. By combining the LP lunar GM (gravitational constant G times mass M) (4902.8003 ± 0.0012 km^3/s^2) with either the GM(Earth + moon) from the Lunar Laser Ranging (LLR) solution of this paper or Earth's GM from artificial satellite ranging, one gets an Earth-moon mass ratio of 81.300566 ± 0.000020 (*28*).

The normalized polar moment of inertia (C/MR^2, where R is the radius) or homogeneity constant for the moon is a measure of the radial density distribution where a value of 0.4 indicates a homogeneous moon and a value less than 0.4 indicates increasing density with depth (for example, Earth with a sizable core has $C/MR^2 = 0.33$). The solution for the three principal moments of inertia $A < B < C$ depends on four relations given by the lunar libration parameters $\gamma = (B - A)/C$ and $\beta = (C - A)/B$, determined from LLR, and the second-degree gravity harmonics $J_2 = [C - (A + B)/2]/MR^2$ and $C_{22} = (B - A)/4MR^2$. The values for the polar moment have varied mostly because of different solutions for the second-degree gravity harmonics. The LLR solution is $C/MR^2 = 0.394 \pm 0.002$ (*29*), and the combination with earlier spacecraft results gives 0.393 ± 0.001 (*30*). A major contribution to published LLR libration parameter uncertainties is from the C_{31} and C_{33} harmonics. An LLR solution with 28 years of data, while adopting the LP values of J_2, C_{31}, and C_{33}, gives $\beta = (631.486 \pm 0.09) \times 10^{-6}$ and $\gamma = (227.871 \pm 0.03) \times 10^{-6}$. The uncertainty in β and γ is mainly due to the size of a possible core. Combining J_2, C_{22}, β, and γ gives the polar $C/MR^2 = 0.3932 \pm 0.0002$ (an uncertainty of five times the formal error) and the average moment $I/MR^2 = 0.3931 \pm 0.0002$ [$I = (A + B + C)/3$]. The uncertainties of J_2 and C_{22} dominate the moment error, although from the improvement of the second-degree harmonics, the resulting uncertainty in C/MR^2 is reduced by about a factor of 5 over previous estimates. J_2 and C_{22} are consistent with β and γ within the stated uncertainty, which is a welcome improvement over sizable discrepancies noted in many historical values (*31*).

The lunar polar moment, when combined with compositional, thermal, and density models of the lunar crust and mantle, can allow some useful inferences to be drawn about the mass and size of a possible metallic core (*32*, *33*). The present determination of C/MR^2 yields an upper bound of 0.3934, only slightly larger than that adopted by Hood and Jones (*32*). Consequently, their conclusion that the most probable core mass lies between 1 and 4% of the lunar mass remains unchanged. For an assumed Fe composition, the core radius would lie between about 300 and 450 km.

Using the model of Binder (*34*) and our value of the moment-of-inertia factor (I/MR^2) of 0.3931 ± 0.0002, we find that the radius of an Fe core is 320 +50/−100 km and its mass is 1.4 +0.8/−0.9% of the moon's mass. The corresponding radius and mass of a FeS core are 510 +80/−180 km and 3.5 +1.9/−2.6%, respectively. If the maximum radius of the core is 450 km as derived from the seismic and magnetic data, then the core is probably Fe or Fe-rich, although an FeS core is not excluded by the data or models.

Although the inferred existence of a small metallic core with mass exceeding 1% of the lunar mass is indirect and provisional, if verified by future direct measurements, such a core would imply that the moon is not composed entirely of terrestrial mantle material. The latter bulk composition would result in an Fe-rich core representing only 0.1 to 0.4% of the lunar mass in order to produce observed depletions of lunar siderophile elements (*35*). In its simplest form, the leading hypothesis for lunar origin, the giant impact model, predicts a moon composed primarily of material from Earth's mantle and the impactor's mantle and, therefore, little or no metallic core (*36*). However, more recent versions of the model in which the giant impact occurred before completion of Earth accretion (*37*) permit the presence of cores in the range inferred here.

References and Notes

1. E. L. Akim, *Dokl. Akad. Nauk SSSR* **170**, 799 (1966).
2. P. M. Muller and W. L. Sjogren, *Science* **161**, 680 (1968). This then new method of determining the gravity was called "line of sight." The Doppler residual, from tracking the spacecraft, measures the velocity in the line-of-sight direction from the tracking station to the spacecraft. The gravity field is found from the Doppler derivative corrected for geometry (mapped to the lunar vertical gravity direction) and spacecraft altitude (downward continued).
3. F. G. Lemoine, D. E. Smith, M. T. Zuber, G. A. Neumann, D. D. Rowlands, *J. Geophys. Res.* **102**, 16339 (1997).
4. M. T. Zuber, D. E. Smith, F. G. Lemoine, G. A. Neumann, *Science* **266**, 1839 (1994).
5. The only polar inclination (i = 90°) orbiters were LO-IV, LO-V, and Clementine. All other spacecraft for which we have data have $i < 30°$. The LO polar orbits, however, were also elliptical with the only low-altitude data near the lunar equator.
6. Unlike the line-of-sight technique, our spherical harmonic models are fully dynamic in that they numerically integrate the equations of motion for the spacecraft accounting for all forces such as the gravity field, perturbations of other planets, solar radiation pressure on the spacecraft, and relativistic terms. Because we process the LP data with intervals or arcs of 2 days, we see the dynamic effect of the farside on 24 orbits at a time. This dynamic effect combined with the dynamic information of the other spacecraft at different inclinations (10° to 30°) and eccentricities gives the total farside gravity we observe.
7. This gravity solution (LP75G), like the previous solution (LP75D), is available from the Geosciences Data Node of the Planetary Data System (pds-geophys.wustl.edu/pds/lunar_prospector) or can be requested from A.K.
8. W. M. Kaula, *Theory of Satellite Geodesy* (Blaisdell, Waltham, MA, 1966).
9. The gravity solution is a least squares determination [see C. L. Lawson and R. J. Hanson, *Solving Least Squares Problems* (Society for Industrial and Applied Mathematics, Philadelphia, PA, 1995)] with the Jet Propulsion Laboratory's Orbit Determination Program (ODP) software [see T. D. Moyer, *JPL Technical Report 32-1527* (Jet Propulsion Laboratory, California Institute of Technology, Pasadena, CA, 1971)].
10. W. M. Kaula, *Science* **166**, 1581 (1969).
11. B. G. Bills and A. J. Ferrari, *J. Geophys. Res.* **85**, 1013 (1980).
12. D. E. Smith, M. T. Zuber, G. A. Neumann, F. G. Lemoine, *ibid.* **102**, 1591 (1997).
13. K. K. Williams and M. T. Zuber, *Icarus* **131**, 107 (1998).
14. P. D. Spudis, R. A. Reisse, J. J. Gillis, *Science* **266**, 1848 (1994).
15. J. Arkani-Hamed, *J. Geophys. Res.* **103**, 3709 (1998).
16. H. J. Melosh and W. B. McKinnon, *Geophys. Res. Lett.* **5**, 985 (1978); S. C. Solomon, R. P. Comer, J. W. Head, *J. Geophys. Res.* **87**, 3975 (1982); S. R. Bratt, S. C. Solomon, J. W. Head, *ibid.* **90**, 12415 (1985).
17. D. U. Wise and M. T. Yates, *J. Geophys. Res.* **75**, 261 (1970).
18. R. J. Phillips, J. E. Conel, E. A. Abbott, W. L. Sjogren, J. B. Morton, *ibid.* **77**, 7106 (1972).
19. S. R. Bratt, S. C. Solomon, J. W. Head, C. H. Thurber, *ibid.* **90**, 3049 (1985).
20. S. C. Solomon and J. W. Head, *ibid.* **84**, 1667 (1979).
21. S. R. Taylor, *Planetary Science: A Lunar Perspective* (Lunar and Planetary Institute, Houston, TX, 1982).
22. G. A. Neumann, M. T. Zuber, D. E. Smith, F. G. Lemoine, *J. Geophys. Res.* **101**, 16841 (1996).
23. J. Arkani-Hamed, *Proc. Lunar Sci. Conf.* **4**, 2673 (1973).
24. J. W. Head, *Rev. Geophys.* **14**, 265 (1976).

25. H. J. Melosh, *Proc. Lunar Sci. Conf.* **9**, 3513 (1978); S. C. Solomon and J. W. Head, *Rev. Geophys.* **18**, 107 (1980); R. J. Willemann and D. L. Turcotte, *Proc. Lunar Planet. Sci.* **12B**, 837 (1981).
26. M. A. Wieczorek and R. J. Phillips, *J. Geophys. Res.* **103**, 1715 (1998).
27. A. B. Kucinskas and D. L. Turcotte, *Icarus* **112**, 104 (1994); A. B. Kucinskas, D. L. Turcotte, J. Arkani-Hamed, *J. Geophys. Res.* **101**, 4725 (1996). For Fig. 1, we used a density of 2.8 g/cm^3 for the crust and 3.3 g/cm^3 for the mantle.
28. The LLR sun/(Earth + moon) mass ratio is 328900.559 ± 0.002, which gives in TDB (Barycentric Dynamical Time) units *GM*(Earth + moon) = 403503.236 ± 0.002 km^3/s^2. The artificial satellite result is *GM*(Earth) = 398,600.4356 ± 0.0008 km^3/s^2 in TDB units [J. C. Ries, R. J. Eanes, C. K. Shum, M. M. Watkins, *Geophys. Res. Lett.* **19**, 529 (1992)].
29. J. O. Dickey *et al.*, *Science* **265**, 482 (1994).
30. J. G. Williams, X. X. Newhall, J. O. Dickey, *Planet. Space Sci.* **44**, 1077 (1996).
31. B. G. Bills, *J. Geophys. Res.* **100**, 26297 (1995).
32. L. L. Hood and J. H. Jones, *ibid.* **92**, 396 (1987).
33. S. Mueller, G. J. Taylor, R. J. Phillips, *ibid.* **93**, 6338 (1988).
34. A. B. Binder, *ibid.* **85**, 4872 (1980).
35. For example, see H. E. Newsom, in *Origin of the Moon*, W. K. Hartmann, R. J. Phillips, G. J. Taylor, Eds. (Lunar and Planetary Institute, Houston, TX, 1986), pp. 203–230.
36. A. G. W. Cameron, *Icarus* **126**, 126 (1997); R. M. Canup and L. W. Esposito, *ibid.* **119**, 427 (1996).
37. A. G. W. Cameron and R. M. Canup, paper presented at 29th Lunar and Planetary Science Conference, Lunar and Planetary Institute, Houston, TX, 16 to 20 March 1998.
38. We thank G. Neumann and M. Zuber for providing the latest lunar topography solutions from Clementine and F. Lemoine for his lunar gravity field and spacecraft model information for processing the Clementine tracking data. Helpful discussions with D. Turcotte are appreciated. LLR solutions were done with the help of D. H. Boggs, and LP data were processed with the help of E. Carranza, D. N. Yuan, and N. Rappaport. The research was carried out by the Jet Propulsion Laboratory, California Institute of Technology, under a contract with NASA.

1 July 1998; accepted 10 August 1998

Lunar Surface Magnetic Fields and Their Interaction with the Solar Wind: Results from Lunar Prospector

R. P. Lin, D. L. Mitchell,* D. W. Curtis, K. A. Anderson, C. W. Carlson, J. McFadden, M. H. Acuña, L. L. Hood, A. Binder

The magnetometer and electron reflectometer experiment on the Lunar Prospector spacecraft has obtained maps of lunar crustal magnetic fields and observed the interaction between the solar wind and regions of strong crustal magnetic fields at high selenographic latitude (30°S to 80°S) and low (~100 kilometers) altitude. Electron reflection maps of the regions antipodal to the Imbrium and Serenitatis impact basins, extending to 80°S latitude, show that crustal magnetic fields fill most of the antipodal zones of those basins. This finding provides further evidence for the hypothesis that basin-forming impacts result in magnetization of the lunar crust at their antipodes. The crustal magnetic fields of the Imbrium antipode region are strong enough to deflect the solar wind and form a miniature (100 to several hundred kilometers across) magnetosphere, magnetosheath, and bow shock system.

The primary objective of the magnetometer and electron reflectometer (MAG/ER) experiment on Lunar Prospector (LP) is to investigate the nature and origin of the moon's magnetic fields. Measurements by early lunar orbiting spacecraft showed that the moon has no global dipole magnetic field (*1*). The discovery of strong stable components of natural remanent magnetization in many of the returned lunar samples (*2*) and the detection of surface magnetic fields of up to hundreds of nanoteslas at the landing sites (*3*) were thus major surprises of the Apollo program. Paleointensity measurements on the returned samples suggest that the lunar surface field was comparable in intensity to the present-day terrestrial surface field from about 3.6 to 3.8 billion years ago (Ga) and about an order of magnitude lower before and after this time period (*4*).

The Apollo 15 and 16 subsatellite magnetometers in low, 100-km-altitude orbits detected regions of crustal magnetic fields of 100-km scale size (*5*), and electron reflection (ER) magnetometry revealed hundreds of magnetic patches on the surface, ranging in size from ≲7 km, the resolution limit of the observations, to ~500 km (*6*). In general, the lunar highlands have stronger fields than the younger maria (*5*, *6*), and there is evidence that some of the far-side basin ejecta are magnetized (*7*). The largest concentrations of surface magnetic fields in the ~20% of the moon sampled by the subsatellites are located within zones centered on the antipodes of the Imbrium, Serenitatis, Crisium, and Orientale impact basins (*8*). These four large circular ringed basins have ages between ~3.85 and 3.6 Ga (*9*), about the same as the most strongly magnetized returned samples. With the exception of a linear magnetic feature that follows the Rima Sirsalis rille (*10*) and a tendency for strong anomalies to occur in association with unusual albedo markings of the Reiner Gamma class (*11*), however, no clear-cut association of surface magnetic fields with surface selenological features was found. Furthermore, the directions of the crustal fields of the >100-km-size regions, as determined by the subsatellite magnetometers, appear to be randomly distributed (*12*). A MAG/ER experiment flown on Mars Global Surveyor recently discovered similar localized patches of surface magnetic fields at Mars, but with surface field strengths ~1000 times as strong (*13*).

The MAG/ER on LP, which is based on instruments flown on Mars Observer (*14*) and Mars Global Surveyor, is designed to map surface magnetic fields with high sensitivity (~0.01 nT at the surface) and spatial resolution (~4 km) over the entire moon (*15*). The MAG measures the vector magnetic field at the spacecraft, and when the external field is steady and plasma disturbances (which can be detected by the ER) are minimal, the lunar crust magnetic field intensity and direction at the spacecraft altitude can be determined by subtracting the external field.

ER magnetometry (*6*) depends on the magnetic mirror effect, that is, the reflection of charged particles from regions of increased magnetic fields. In a uniform field the particles move along helical paths of constant pitch angle (α, the angle between the particle velocity and the magnetic field direction) and radius (called the gyro-radius). However, if the field strength increases in the direction of motion as the surface is approached, particles with pitch angles greater than a cutoff pitch angle (α_c) will be reflected back along the lines of force, whereas those with pitch angle below α_c will impact the surface and be lost. The cutoff pitch angle depends on the ratio of the total field strength at the surface to that at the spacecraft. A technique for identifying

R. P. Lin, Space Sciences Laboratory and Physics Department, University of California, Berkeley, CA 94720, USA. D. L. Mitchell, D. W. Curtis, K. A. Anderson, C. W. Carlson, J. McFadden, Space Sciences Laboratory, University of California, Berkeley, CA 94720, USA. M. H. Acuña, NASA Goddard Space Flight Center, Greenbelt, MD 20771, USA. L. L. Hood, Lunar and Planetary Laboratory, University of Arizona, Tucson, AZ 85721, USA. A. Binder, Lunar Research Institute, Gilroy, CA 95020, USA.

*To whom correspondence should be addressed. E-mail: mitchell@ssl.berkeley.edu